Topaz from Mason County, Texas

Roy Bassoo, Diane Eames, Matthew F. Hardman, Kenneth Befus, and Ziyin Sun

Gem-quality naturally blue topaz occurs in Mason County, Texas. Known as "Texas topaz," this gem is highly sought after in the United States because of its domestic provenance and rare natural blue color. To date, no studies have identified gemological or compositional characteristics that could distinguish Texas topaz from topaz sourced elsewhere. This study provides a historical account of topaz from Mason County and discusses its geologic origin, compositional characteristics, manufacture, and significance to the gem trade. A total of 83 alluvial topaz crystals from Mason County were analyzed using standard gemological testing; Fourier-transform infrared, ultraviolet/visible/near-infrared, and Raman spectroscopic techniques; and laser ablation–inductively coupled plasma–mass spectrometry to gather gemological and geochemical data. Most Texas topaz is colorless, though some is light blue or brown. A small percentage of the blue stones displayed a saturated bodycolor. Color zoning was often visible and became more noticeable with luminescent excitation. Ultraviolet luminescence at 225 nm excitation revealed green to blue luminescent growth bands and rarely red luminescent growth bands. Topaz crystals from Mason County are not often free of inclusions. When present, multiphase melt and fluid inclusions contain carbon dioxide. Mineral inclusions include albite, anorthite, quartz, muscovite, pseudobrookite, and columbite-tantalite. Machine learning algorithms were applied to fingerprint the trace element composition of the samples. Trace concentrations of phosphorus, scandium, titanium, iron, gallium, germanium, niobium, tin, tantalum, and tungsten best constrained the formation and provenance of Texas topaz. For gemologists, these trace elements can also aid in assessing the geographic provenance because most Texas topaz presents a distinct trace element composition. This work demonstrates the potential effectiveness of machine learning and statistical modeling in gemstone provenance determination. These can be powerful tools in conjunction with traditional gemological discrimination techniques.

Topaz is an orthorhombic nesosilicate with the general chemical formula $Al_2SiO_4F_2$. It can form from fluorine- and lithium-rich, peraluminous (aluminum-rich and calcium-poor), and highly fractionated silicic melts or gases geologically associated with rhyolites, pegmatites, or hydrothermal-greisen rocks (Burt et al., 1982; Congdon and Nash, 1988; Payette and Martin, 1990; Menzies, 1995; Zhang et al., 2002; Marshall and Walton, 2007; Gauzzi et al., 2018; Gauzzi and Graça, 2018). In pegmatites, topaz is found alongside quartz, feldspar, muscovite, and accessory tourmaline and fluorite (Pollard et al., 1989). In greisens, which are granitic rocks altered by internal magmatic fluids, topaz is also associated with rare metal deposits of tantalum, niobium, tungsten, lithium, tin, and molybdenum (Burt et al., 1982; Manning and Hill, 1990; Taylor, 1992; Raimbault et al., 1995; Charoy and Noronha, 1996; Williams-Jones et al., 2000).

In Brief

- This study discusses the history, geologic origin, compositional characteristics, manufacture, and significance within the trade of naturally blue Texas topaz.
- Trace concentrations of tin and tungsten in Texas topaz and the presence of cassiterite and scheelite in the region suggest possible greisen ore mineralization in Mason County, Texas.
- Machine learning and statistical modeling of topaz trace element data from worldwide sources demonstrate their utility in assisting with gemstone provenance determination.

Globally sourced gem and fine mineral specimens of topaz are prized for their luster, clarity, hardness, and wide range of colors, including orange, pink, and blue. Whereas most topaz is colorless, certain growth

See end of article for About the Authors and Acknowledgments.
Gems & Gemology, Vol. 59, No. 4, pp. 414–431,
http://dx.doi.org/10.5741/GEMS.59.4.414

Figure 1. A fine 925 ct crystal that was formerly displayed in the Texas State Capitol and sat on the governor's desk in 1969 when the legislature adopted blue Texas topaz as the state gem. This specimen was found in 1904 and now resides in the Hamman Gem and Mineral Gallery in the Department of Earth and Planetary Sciences at the University of Texas at Austin (catalog no. B0344). Photo by Blanca Espinoza.

environments induce defects and impurities that create color centers. In the case of pink to violet colors, Cr^{3+} acts as a chromophore, substituting for Al^{3+}. A combination of oxygen-to-metal charge transfer and radiation-induced color centers can modify pink to violet material to orange Imperial topaz (Gaft et al., 2003; Schott et al., 2003; Taran et al., 2003). Oxygen hole center defects produce brown or blue colors, though the possibility of additional defects causing blue color remains uncertain (Krambrock et al., 2007; Rossman, 2011). Pronounced blue colors can also be created or enhanced through irradiation and heat treatments (Simmons, 2007). Colorless topaz was first irradiated to create a blue color in 1957 (Pough, 1957). Artificially irradiated and heat treated blue topaz subsequently entered the market in the late 1970s, and its popularity and low cost eventually made it the most commonly irradiated gemstone on the market (Nassau and Prescott, 1975; Crowningshield, 1981; Nassau, 1985). This treatment became so widespread that any blue topaz in today's market is assumed to have been irradiated (Rossman, 2011).

Considering the prevalence of artificially blue topaz, the naturally blue topaz from Mason County, Texas, is significant (figure 1). Indeed, faceters of Texas topaz understand that treating this gemstone could render it indistinguishable from those found in other locations. In Mason County, as with most geographic occurrences, colorless topaz is the most common. However, faint blue to sky blue hues can be relatively uncommon. Pink, brown, and gray colors are rare (figure 2).

Topaz was first collected in Mason County in the late 1800s, long before the first reported accounts of topaz treatment (Meyer, 1913; Leiper, 1951). By the 1950s, Texas topaz had become important in the regional gem trade (White, 1960; Towner, 1968, 1969; Browne, 1982). The timing is anecdotally linked to World War II, when scientists moved to the American Southwest for the nuclear weapons program and engaged in recreational mineral hunting on weekends and holidays. This led to the formation of gem and mineral groups and increased rockhounding and gem faceting in the region. Topaz from Mason County be-

Figure 2. Rough topaz from Mason County analyzed in this study, showing the range of color of this material. The large blue specimen weighs 188 ct. Photo by Emily Lane; courtesy of Diane Eames.

came the most commonly used gemstone in faceting competitions at Texas gem and mineral shows. In 1969, the state legislature adopted Mason County blue topaz as the official state gemstone, introducing the "Texas topaz" label.

Texas topaz remained in the hobbyist realm until the early 2000s, when Diane Eames and Brad Hodges established Gems of the Hill Country, a jewelry store in the town of Mason. From this rural platform they built a successful niche jewelry business centered on locally sourced and manufactured Texas topaz pieces (figure 3). Gems of the Hill Country supplied both local and national markets with jewelry showcasing Texas topaz. Their advertising campaign significantly elevated the prestige of Texas's state gemstone.

Because of its local provenance, topaz from Texas has a much higher regional value than similarly colored topaz from other localities worldwide. The most sought-after stones exhibit a saturated blue color. Price varies with the saturation of blue color and the cut quality. Early in the twentieth century, faceters used the Portuguese cut to create stones with deep pavilions to intensify the pale colors. Today most of this topaz is faceted in the Lone Star cut (box A) or variations thereof. Blue or brown color zones are placed in the culet to intensify the perceived color (King Jr., 1961).

Establishing the provenance of Texas topaz has posed a challenge in the regional gem trade. Buyers are wary of intentional or inadvertent substitution of low-value foreign topaz for high-value local material. This article presents a gemological and analytical

Figure 3. Faceted Texas topaz specimens with brown, blue, and green bodycolors, ranging from 0.62 to 9.34 ct. Texas topaz has been sought after for its naturally occurring blue color. Photo by Brad Hodges; courtesy of Diane Eames.

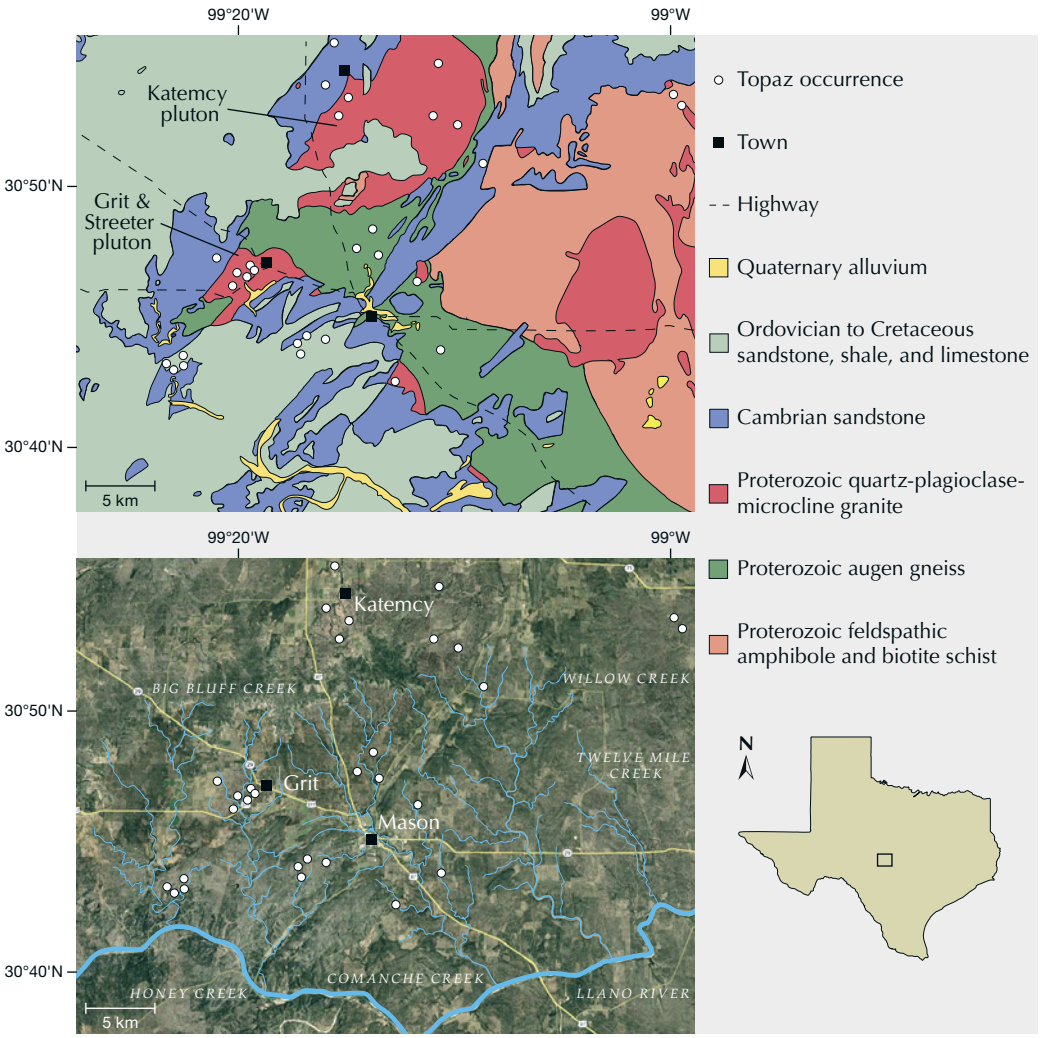

Figure 4. Geologic map (top) and aerial view (bottom) of the Mason County area in Texas, showing known locations where topaz has been collected in alluvium. While many Texas topaz occurrences have been discovered historically, these maps document those that have been published (Leiper, 1951; Towner, 1968, 1969; Fechenbach, 1984). The geologic map is modified from the Geologic Database of Texas (https://txpub.usgs.gov/txgeology).

study of Texas topaz to augment the various worldwide databases of colored stone deposits. Trace element compositions for topaz from Mason County are presented, along with a demonstration of how machine learning can assist with the geographic provenance determination of Texas topaz.

GEOLOGY AND MINING

Texas topaz crystallizes from niobium-yttrium-fluorine (NYF) pegmatites that are genetically and spatially associated with granites in the Llano Uplift in central Texas. The Llano Uplift is a 9000 km^2 exposure of Proterozoic igneous and metamorphic rocks from the Grenville orogen that are 1.0 to 1.3 billion years old (Mosher et al., 2008). Topaz can be found in pegmatites throughout the Llano Uplift; however, nearly all gem-quality material is derived from the granitic Grit, Streeter, and Katemcy plutons in the western Llano Uplift (White, 1960; Towner, 1969; Reed, 1999; Barker and Reed, 2010). The source granites have very low strontium concentrations and zirconium/hafnium ratios, suggesting that extreme fractional crystallization rather than partial melting led to their formation (Barker and Reed, 2010; Collins, 2008). The topaz-producing granites intrude the Proterozoic Packsaddle schist, Valley Springs gneiss, and/or other granite plutons. When not exposed, they are mostly overlain by the Middle Cambrian Hickory sandstone member of the Riley Sandstone formation, Cretaceous Edwards limestones, and quaternary alluvium (figure 4).

Euhedral topaz crystallizes in sub-meter-diameter vugs within relatively small meter- to decameter-long pegmatites, which tend to be gradational with the host granites (White, 1960). Pegmatite vugs also contain microcline, albite, and "books" of biotite, fluorite, and quartz embedded within a clay matrix (Meyer, 1913; Leiper, 1951; Hoover, 1992). Topaz has

BOX A: CUTTING OF TEXAS TOPAZ

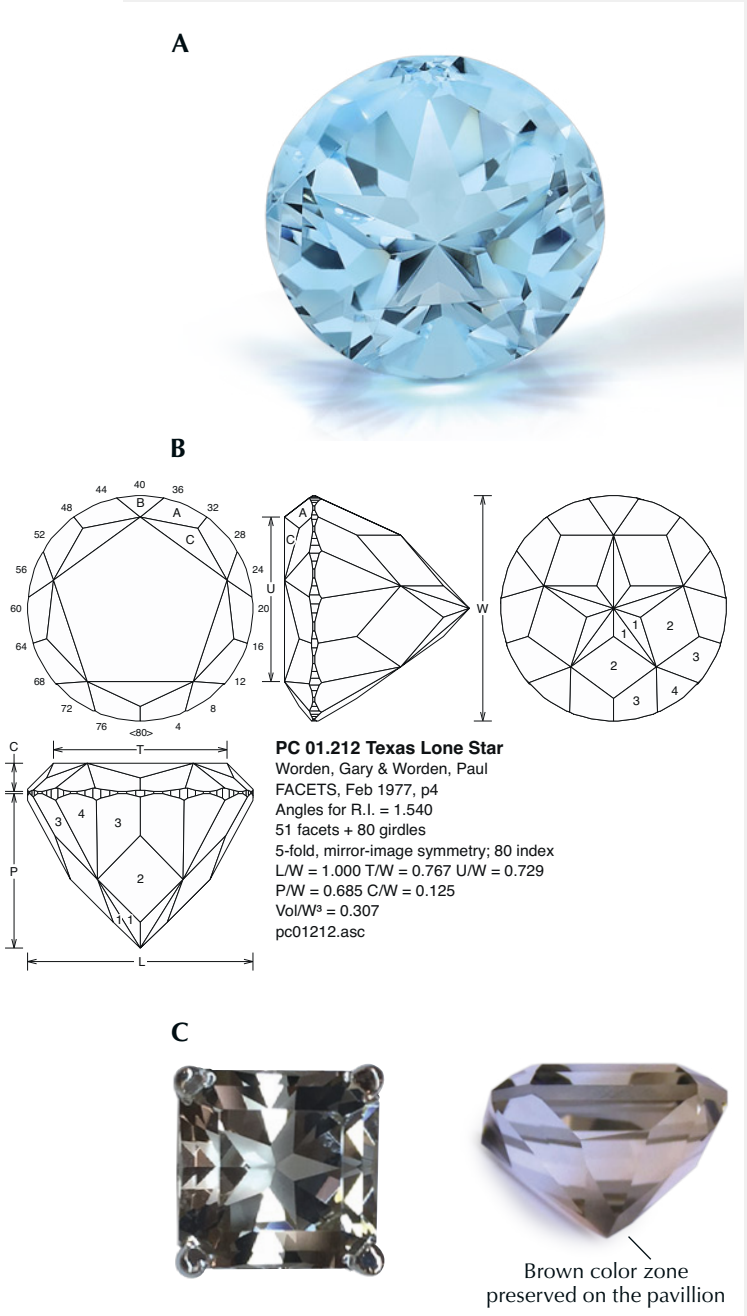

Figure A-1. A: 14.5 mm round 13.8 ct topaz from Mason County, Texas. Photo by Blanca Espinoza; courtesy of Form to Feeling. B: Facet design for Lone Star cut (from the open database at http://www.facetdiagrams.org). C: A cut topaz with brown color zones deliberately positioned along the pavilion to display a brownish bodycolor in the table view. Photos by Brad Hodges.

Topaz is popular with American faceters for its perfect basal cleavage plane. To prevent breakage during faceting and scratches during polishing, a gem cutter must avoid placing the table along the cleavage plane. Chips along the girdle may indicate that the cleavage plane is parallel to the girdle, which is also undesirable. The strongest color saturation in topaz occurs parallel to the *c*-axis. Therefore, faceters cannot simply orient the stone away from potential weakness associated with the basal cleavage without sacrificing color. To optimize color and avoid structural weakness, faceters attempt to cut topaz so that the table is ~7° off the cleavage plane, an orientation that minimizes fractures and accentuates color. A Texas topaz faceted with a 0.5 micron polish and a correctly oriented cleavage plane can achieve subadamantine luster and deeply saturated color, both of which contribute to its appeal.

The development of the Lone Star cut (figure A-1, A) distinguished Texas topaz as a regionally unique and desirable gemstone. The facets on its pavilion produce a large five-point star visible through the table, a shape reminiscent of the star in the Texas state flag. The pavilion of the traditional Lone Star cut represents up to 80% of the stone's total depth, making it unsuitable for rings and earrings. Alternative versions have a pavilion that accounts for 60–65% of the total depth, and these have become popular. Most are cut as round gems, but fancy Lone Star variations have also been developed.

Several Texas faceters have contributed to the design and popularity of the Lone Star cut. Gary Worden and Paul Worden of San Angelo are credited as the original designers (Worden, 1977; see figure A-1, B). Additional star cuts were developed by hobbyist faceters. The most influential were Charles Covill and Robert Strickland, both of Austin, who developed many variations and freely shared their designs with other gem cutters.

The commercial development of Lone Star cut Texas topaz initially relied on independent hobby cutters mainly selling their work in the town of Mason. With the opening of the retail store Gems of the Hill Country in 2007, manufacturing shifted to a commercial scale. Cofounders Diane Eames and Brad Hodges sourced, faceted, and designed Texas topaz jewelry pieces, providing a retail avenue for the state gem. Acquiring topaz from local rock hounds, ranchers, and topaz enthusiasts, Gems of the Hill Country expanded its inventory of gem-quality blue, pink, and brown topaz (figure A-1, C). Gems of the Hill Country has since closed, but the founders still maintain a large inventory of Texas topaz. During its decade-plus run, Gems of the Hill Country not only sold Texas topaz to buyers in the United States, Germany, and the United Kingdom but also founded and participated in Texas Topaz Day in Mason from 2008 to 2012, celebrating Texas topaz with a public mineral hunt on local topaz-bearing ranches. These efforts elevated the awareness and prestige of Texas topaz and "American-made" gemstones and jewelry.

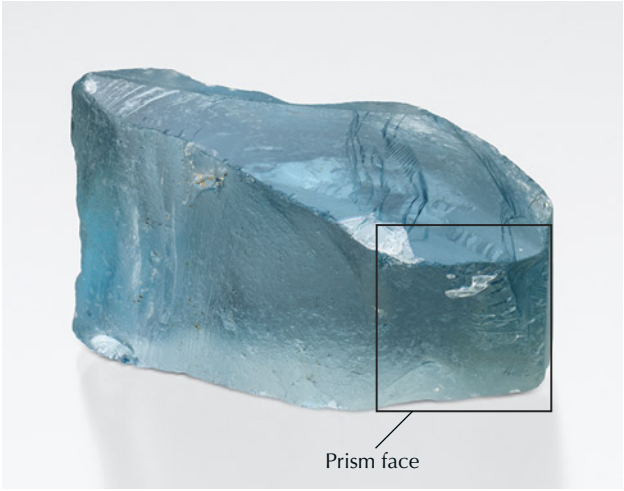

Figure 5. Example of a waterworn topaz with terminations and prism faces with narrow grooves and etchings in a 188 ct specimen. Photo by Emily Lane; courtesy of Diane Eames.

only rarely been extracted directly from vuggy pegmatites of Mason County granites through small hard-rock mining operations. Primary topaz extracted from these pegmatite vugs typically presents as rhombic to square and singly terminated prisms. As shown in figure 1 and figure 5, terminations and prism faces may display narrow grooves and etchings (White, 1960).

The vast majority of Texas topaz has been recovered from alluvial drainages, specifically along creeks and rivers south and east of the Katemcy pluton. These localized drainages sometimes correspond with the trend of pegmatites. Liberated alluvial topaz accumulates within potholes, depressions, and other structural traps where stream velocities slow, causing the high-density topaz (~3.5 g/cm^3) to settle (figure 6, top). Some alluvial topaz remains euhedral yet frosted, but most are well rounded and abraded. Corundum, including ruby, has occasionally been found within topaz-bearing alluvium, though it likely did not form alongside topaz. The original economic target for prospectors in Mason County was cassiterite, a tin ore mineral (Leiper, 1951; Sparks, 1968). Alluvial topaz is also found in the Middle Cambrian Hickory Sandstone Formation (White, 1960; Sparks, 1968; Fechenbach, 1984; Barnes et al., 1992; Collins, 2008). The occurrence of alluvial topaz in both Holocene and Middle Cambrian sedimentary rocks suggests a protracted history of erosion and deposition across millions of years.

Mining in central Texas has a rich history that began with the Spanish conquistadors searching for riches, including gold and the famed Seven Cities of Cibola. In 1893, George Kunz published the first report of topaz in Texas (Kunz, 1893). At that time, pegmatites in the Llano Uplift were being carefully assessed for their economic potential, as some hosted exceptional minerals containing rare earth elements.

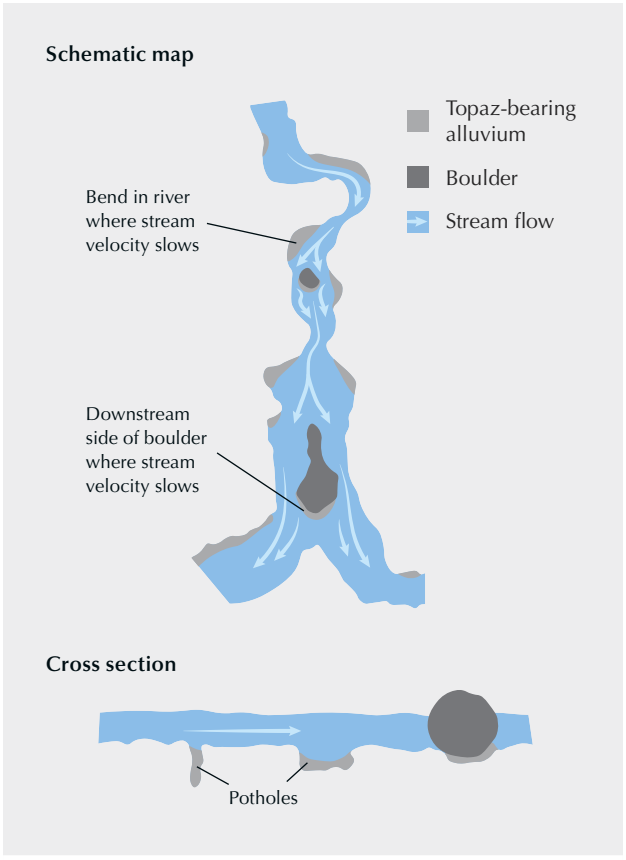

Figure 6. Top: Schematic map and cross section views of representative locations where alluvial topaz accumulates along a river or stream. Modified from Fechenbach (1984). Bottom: Dalan Hargrave (background) and Diane Eames (foreground) sieving gravels for topaz. Photo by Brad Hodges.

Thomas Edison's Piedmont Mining Company purchased the Barringer Hill pegmatite deposit to acquire rare earth minerals such as gadolinite, which were critical for filaments in the emerging technology of light bulbs (Smith, 2008). This acquisition did not involve topaz, however, as the rare earth pegmatites tended to occur in the eastern Llano Uplift and gem-quality topaz was found much farther to the west. Economic interest in the topaz-bearing pegmatites was later fueled by the search for economic tin deposits because of their association with cassiterite (Meyer, 1913).

Prospecting for topaz in Mason County has primarily been a seasonal activity by part-time local artisanal miners and recreational rock hounds (e.g., Browne, 1982; International Labour Organisation, 1999; Hinton, 2005). Prospectors sift gravels along waterways on public lands or local ranches such as the Seaquist or Lindsay ranches that allow prospecting for a daily fee (figure 6, bottom). The most productive sites are placers at the contact between bedrock and stream deposits. When prospective locations for alluvial topaz are determined, the sediment is disaggregated and passed through sieves. Published anecdotes refer to placer "pockets" containing dozens of stones larger than 1 cm in diameter and others with multiple waterworn crystals ranging from 8 to 926 ct. Mason County has produced topaz crystals and alluvial stones weighing less than 1 ct up to approximately 6800 ct, which is the largest topaz ever recovered in North America (Leiper, 1951; White, 1960; Towner, 1968, 1969; Sparks, 1968; Sinkankas, 1997). Historically, the average size recovered by artisanal and recreational prospectors has been between 1 and 10 ct. Decades of targeted placer mining on publicly accessible tracts of land have considerably depleted these deposits, as the authors can attest to after many laborious hours digging in Mason County drainages.

Topaz is still found today but in far lesser abundance than in earlier decades. Many areas that appear untouched today were likely excavated by past miners and have subsequently been refilled with gravels during flooding events. Rounded and abraded topaz may be mistaken for quartz. However, topaz can be accurately identified by its habit, cleavage, coloration, clarity, frosted appearance, and high density. Prospectors in the past sometimes carried bromoform or other heavy liquids to isolate the heavier topaz from the lighter quartz (Towner, 1968, 1969). Most prospectors work during the day, but others use UV flashlights at night to find strongly luminescent specimens.

MATERIALS AND METHODS

A total of 71 rough Texas topaz specimens were loaned to GIA for study by author DE, and an additional 12 rough samples were loaned to GIA by the Barron Gem and Mineral collection in the Department of Earth and Planetary Sciences at the University of Texas at Austin. Topaz specimens from other global localities were sourced from GIA's colored stone reference collection and are summarized in table 1. These samples are of D-type and E-type origin according to GIA's classification scheme for degree of confidence of origin (Vertriest et al., 2019). These 379 samples total are from Australia (8), Brazil (89), Colombia (47), Germany (3), Guyana (107), Japan (1), Mexico (40), Namibia (3), Nigeria (5), Pakistan (4), Russia (9), Sri Lanka (4), the United States (excluding Texas, 30), and Zimbabwe (29). Topaz samples with Texas listed as their origin are confirmed to be from Texas. The authors acknowledge that mineral specimens not sourced from Texas might be ambiguous in origin, and we consider the nuances in their trace element concentrations beyond the scope of this study. Instead, this study presents a potential use of machine learning to assist specifically in provenance determinations of Texas topaz.

Morphology, optical character, inclusion species, and composition of Texas topaz were assessed using various gemological, spectroscopic, and analytical methods. We also calculated specific gravity by measuring the mass in air and the mass submerged in water using a Mettler AM100 scale. A Gem Instruments Duplex II refractometer was used to measure refractive index. Surface fluorescence images were acquired using a DiamondView ultraviolet imaging system with a flash lamp source, an incident wavelength of ~225 nm, and an exposure time of approximately 5 s. Visible/near-infrared (Vis-NIR) absorption spectra were collected with a PerkinElmer Lambda 950 UV-Vis spectrophotometer in the 200–1000 nm range, with 1 nm spectral resolution at 77 K. Bulk Fourier-transform infrared (FTIR) spectra were collected using a Thermo Scientific Nicolet iN10 FTIR spectrometer equipped with an XT-KBr beam splitter and a mercury-cadmium-telluride (MCT) detector operating with a 4× beam condenser. FTIR analyses were performed across the 675–4000 cm^{-1} range in cooled transmission mode using a 200 × 200 µm aperture, 64 to 128 scans, and a spectral resolution of 4 cm^{-1}. Raman spectra of topaz-hosted inclusions were collected with a Thermo Scientific DXR Raman microscope equipped with a 532 nm laser operating at 8 mW, a ~2 µm spot, and a high-resolution grating (1800

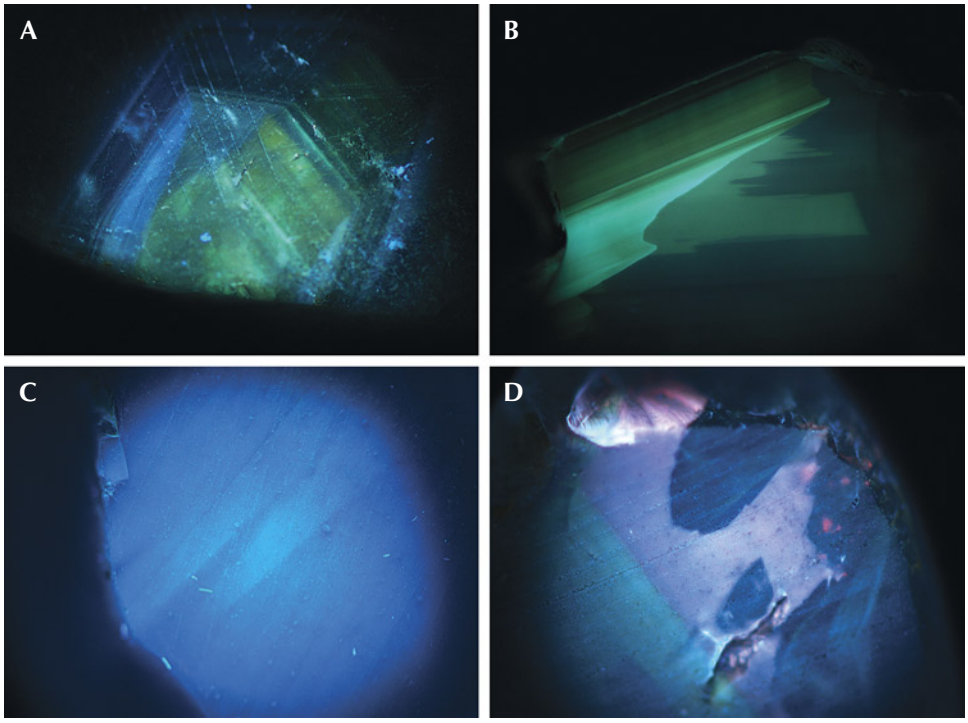

Figure 7. Representative UV luminescence images of Texas topaz acquired using ~225 nm excitation. Note the red luminescent zones in a topaz sample with elevated levels of chromium (image D). Images by Roy Bassoo; field of view ~15 mm.

lines/mm). Inclusion identity was confirmed with Raman spectra by matching peak positions and heights of the inclusions' spectra with those in the RRUFF spectral database (Lafuente et al., 2016).

Trace element concentrations were measured by laser ablation–inductively coupled plasma–mass spectrometry (LA-ICP-MS) using a Thermo Fisher iCAP Qc ICP-MS, coupled to an Elemental Scientific Lasers NWR213 laser ablation system with a frequency-quintupled Nd:YAG laser (213 nm wavelength with 4 ns pulse width). Ablation was carried out with 55 µm spot sizes, a fluence of 8–10 J/cm^2, repetition rates of 20 Hz, and dwell times of 35 s. The isotope ^{29}Si was used as an internal standard at 152854 ppmw, which is a representative average silicon ppmw content of topaz (Agangi et al., 2014, 2016; Gauzzi et al., 2018). United States Geological Survey glass standards GSD-1G and GSE-1G and National Institute of Standards and Technology (NIST) glass standard SRM 610 were used as external standards. Concentrations are reported as ppm throughout this article. Conversion factors are determined by factory-set parameters of Thermo Scientific's Qtegra software (Version 2.10.3324.131).

In this study, we calibrated a random forest machine learning model (Breiman, 2001) to predict topaz provenance using trace element compositions. This classification model calculated the probability of a single topaz specimen originating from Mason County, Texas. To calibrate this model, two outcome classes were defined: (1) topaz derived from Texas and (2) topaz derived from all other worldwide localities. For detailed information about the parameters used for model calibration, see appendix 1 (www.gia.edu/doc/winter-2023-texas-topaz-appendix1.pdf).

RESULTS

Gemological and Spectroscopic Characteristics. This study examined 83 topaz samples from Mason County ranging in size from 4 to 189 ct, with a mean weight of 21 ct. All of these samples were rounded and abraded and either colorless (47%), blue (50%), or yellowish brown (3%). Of the blue topaz, 75% were very light blue and 19% were light blue with saturated blue color zones. In some instances, this blue color can be desaturated by sunlight (Leiper, 1951). Only 6% of the Texas topaz samples had the deeply saturated blue bodycolor or color zones shown in figure 1. We measured a mean specific gravity of 3.55 ± 0.17 and a mean refractive index of 1.620 ± 0.001 and range from 1.615–1.625. The samples also had a vitreous luster and a white streak.

When exposed to ultraviolet luminescence, the Texas topaz displayed blue and/or green luminescent bodycolor and growth bands (figure 7, A–C). One sample showed red luminescent growth bands (figure 7D), which are known to be caused by Cr^{3+} impurities, which may impart a pink bodycolor (Petrov et

TABLE 1. Summary of trace element concentrations (in ppmw) of topaz measured by LA-ICP-MS.

Locality	Tectonic environment[a]	No. of measurements[b]		P	Sc	Ti	V	Cr	Fe	Ga	Ge	Nb	Sn	Ta	W
U.S. (Texas)	Orogen	180	Min	bdl[c]	1.5	bdl	bdl	bdl	bdl	1.02	12.3	bdl	bdl	bdl	bdl
			Max	589	4.4	209	40.21	99.6	193	17.50	223.7	4.36	2.4	4.100	0.98
			Median	14	3.4	8	bdl	bdl	35	5.57	68.3	0.03	bdl	0.010	bdl
			MAD[d]	7	0.3	4	—	—	24	1.64	23.4	0.03	—	0.010	—
Australia	Orogen	15	Min	bdl	2.1	2	bdl	bdl	10	1.89	12.3	bdl	bdl	bdl	bdl
			Max	153	3.5	44	18.76	4.1	132	9.31	336.3	0.60	1.4	0.050	2.90
			Median	26	3.0	10	bdl	bdl	68	5.46	32.4	0.01	bdl	0.010	bdl
			MAD	15	0.4	5	—	—	33	1.18	8.6	0.01	—	0.010	—
Brazil	Shield	200	Min	bdl	1.3	2	bdl	bdl	bdl	0.40	3.7	bdl	bdl	bdl	bdl
			Max	690	7.7	195	133.65	565.4	4032	25.72	976.2	4.58	19.4	4.240	13.83
			Median	19	2.5	14	9.30	54.7	34	4.25	31.3	bdl	bdl	bdl	bdl
			MAD	10	1.0	11	13.78	81.1	23	4.20	28.0	—	—	—	—
Colombia	Shield	98	Min	bdl	1.6	3	bdl	bdl	bdl	1.74	47.2	bdl	bdl	bdl	bdl
			Max	316	2.8	45	0.70	2.1	105	12.16	239.6	4.08	3.6	15.060	0.72
			Median	34	2.3	10	bdl	bdl	44	4.28	99.9	0.04	bdl	0.020	bdl
			MAD	34	0.4	5	—	—	10	1.49	13.9	0.03	—	0.015	—
Germany	Extended crust	6	Min	12	2.8	8	5.36	4.7	18	0.72	8.1	bdl	bdl	bdl	bdl
			Max	265	3.3	90	20.96	103.4	92	14.48	129.9	0.51	0.4	0.120	0.32
			Median	60	3.3	35	12.28	61.5	25	1.92	62.9	bdl	bdl	bdl	bdl
			MAD	63	0.1	28	7.17	29.2	9	0.96	59.3	—	—	—	—
Guyana	Shield	165	Min	bdl	1.5	11	bdl	bdl	bdl	1.90	6.6	bdl	bdl	bdl	bdl
			Max	3378	130.0	19767	108.00	217.3	1709	52.25	202.0	72.60	32.2	10.320	83.18
			Median	411	8.1	89	0.28	bdl	32	7.21	33.9	0.93	0.2	0.310	0.37
			MAD	421	7.0	84	0.42	—	19	2.88	13.0	1.32	0.3	0.460	0.49
Japan	Orogen	2	Min	46	3.0	2	bdl	0.4	10	5.00	19.2	0.02	0.4	0.010	bdl
			Max	54	3.2	7	bdl	0.4	15	5.77	72.9	0.03	0.6	0.020	0.06
			Median	50	3.1	5	bdl	0.4	12	5.39	46.0	0.03	0.5	0.015	0.03
			MAD	6	0.2	3	—	0.0	4	0.57	39.8	0.01	0.1	0.007	0.04
Mexico	Orogen	80	Min	bdl	2.9	24	bdl	bdl	65	2.71	13.4	0.41	bdl	0.050	0.26
			Max	146	35.3	372	0.69	27.5	2024	41.34	38.1	199.00	4.0	24.330	26.84
			Median	17	5.8	104	0.16	bdl	251	8.75	26.1	2.76	0.2	0.680	1.05
			MAD	5	1.0	35	0.08	—	76	2.41	3.5	1.56	0.2	0.520	0.56
Namibia	Shield	6	Min	12	2.4	1	bdl	bdl	bdl	2.59	44.9	bdl	bdl	bdl	bdl
			Max	93	3.0	16	0.15	bdl	26	8.67	160.9	0.06	bdl	0.010	0.07
			Median	14	2.7	9	bdl	bdl	23	3.27	89.8	bdl	bdl	0.010	bdl
			MAD	3	0.2	9	—	—	4	0.60	63.4	—	—	—	—
Nigeria	Shield	10	Min	bdl	2.6	2	bdl	bdl	21	1.41	18.5	bdl	bdl	bdl	bdl
			Max	106	5.1	198	0.50	6.4	227	9.10	269.0	3.55	bdl	0.470	3.03
			Median	33	3.3	4	bdl	bdl	47	2.00	34.6	0.02	bdl	0.005	bdl
			MAD	26	0.4	3	—	—	30	0.47	12.6	0.02	—	0.007	—

TABLE 1 (continued). Summary of trace element concentrations (in ppmw) of topaz measured by LA-ICP-MS.

Locality	Tectonic environment[a]	No. of measurements[b]		P	Sc	Ti	V	Cr	Fe	Ga	Ge	Nb	Sn	Ta	W
Pakistan	Orogen	10	Min	bdl	2.3	9	bdl	0.4	bdl	1.17	12.2	bdl	bdl	bdl	bdl
			Max	24	3.0	150	44.13	108.2	13	3.61	184.1	0.05	1.0	0.010	0.14
			Median	11	2.8	43	22.44	62.4	bdl	1.62	18.1	bdl	bdl	bdl	bdl
			MAD	10	0.3	40	14.15	53.3	—	0.60	8.1	—	—	—	—
Russia	Orogen	18	Min	11	2.2	6	bdl	bdl	bdl	0.24	0.4	bdl	bdl	bdl	bdl
			Max	954	3.7	121	688.05	1326.8	56	7.06	18.8	0.03	bdl	0.010	0.10
			Median	23	3.0	14	115.95	257.6	bdl	1.17	5.4	bdl	bdl	bdl	bdl
			MAD	10	0.2	10	123.00	277.5	—	0.97	4.9	—	—	—	—
Sri Lanka	Shield	8	Min	bdl	1.9	3	bdl	bdl	bdl	1.68	8.2	bdl	bdl	bdl	bdl
			Max	75	2.9	17	24.78	72.0	138	10.19	123.9	0.15	bdl	0.050	0.08
			Median	bdl	2.4	10	bdl	bdl	35	7.41	83.8	0.05	bdl	bdl	0.04
			MAD	—	0.5	4	—	—	32	3.13	52.8	0.05	—	—	—
U.S. (California)	Orogen	5	Min	10	2.5	2	bdl	bdl	bdl	1.13	243.7	bdl	bdl	bdl	bdl
			Max	30	2.9	20	bdl	bdl	bdl	7.13	420.4	0.08	bdl	0.320	bdl
			Median	13	2.7	3	bdl	bdl	bdl	3.44	373.7	bdl	bdl	0.020	bdl
			MAD	13	2.7	3	—	—	—	3.44	46.7	—	—	0.020	—
U.S. (Colorado)	Orogen	2	Min	48	1.8	3	bdl	bdl	35	1.35	71.6	bdl	bdl	bdl	bdl
			Max	72	2.0	3	0.08	bdl	36	1.83	77.0	bdl	bdl	bdl	bdl
			Median	—	—	—	—	—	—	—	—	—	—	—	—
			MAD	—	—	—	—	—	—	—	—	—	—	—	—
U.S. (Indiana)	Shield	2	Min	192	2.4	12	0.09	bdl	90	11.33	76.5	0.06	bdl	0.030	0.22
			Max	216	2.6	16	0.11	bdl	106	12.86	81.2	0.08	0.3	0.040	0.23
			Median	—	—	—	—	—	—	—	—	—	—	—	—
			MAD	—	—	—	—	—	—	—	—	—	—	—	—
U.S. (Utah)	Orogen	50	Min	bdl	1.9	10	bdl	bdl	35	1.39	8.9	bdl	bdl	bdl	bdl
			Max	142	23.9	996	26.88	191.4	1631	18.52	47.9	96.15	4.5	16.910	40.06
			Median	17	4.1	140	0.14	bdl	226	4.88	19.5	1.76	bdl	0.250	0.46
			MAD	7	0.8	43	0.05	—	92	2.23	2.8	1.33	—	0.210	0.45
Zimbabwe	Shield	58	Min	bdl	1.3	bdl	bdl	bdl	bdl	0.26	138.6	bdl	bdl	bdl	bdl
			Max	322	2.7	42	0.81	59.2	331	4.62	1308.0	0.68	8.7	1.230	0.19
			Median	98	2.4	4	bdl	bdl	bdl	2.86	724.0	0.02	bdl	0.035	bdl
			MAD	107	0.2	3	—	—	—	1.02	484.1	0.03	—	0.037	—
Detection limit (ppmw)				9	0.1	1	0.06	0.3	7	0.02	0.4	0.01	0.2	0.004	0.03

[a]*Classes derived from Simmons et al. (2012).*
[b]*Includes replicate analyses. Please see appendix 1.*
[c]*bdl = below detection limit*
[d]*MAD = median absolute deviation*

al., 1977; Taran et al., 1994, 2003). Only 4% of the analyzed topaz were inert or showed no luminescence response. The UV, visible, and infrared absorbance spectroscopic characteristics of Texas topaz were documented (figure 8). Absorption in the ultraviolet to visible spectrum found that 74% of the ana-

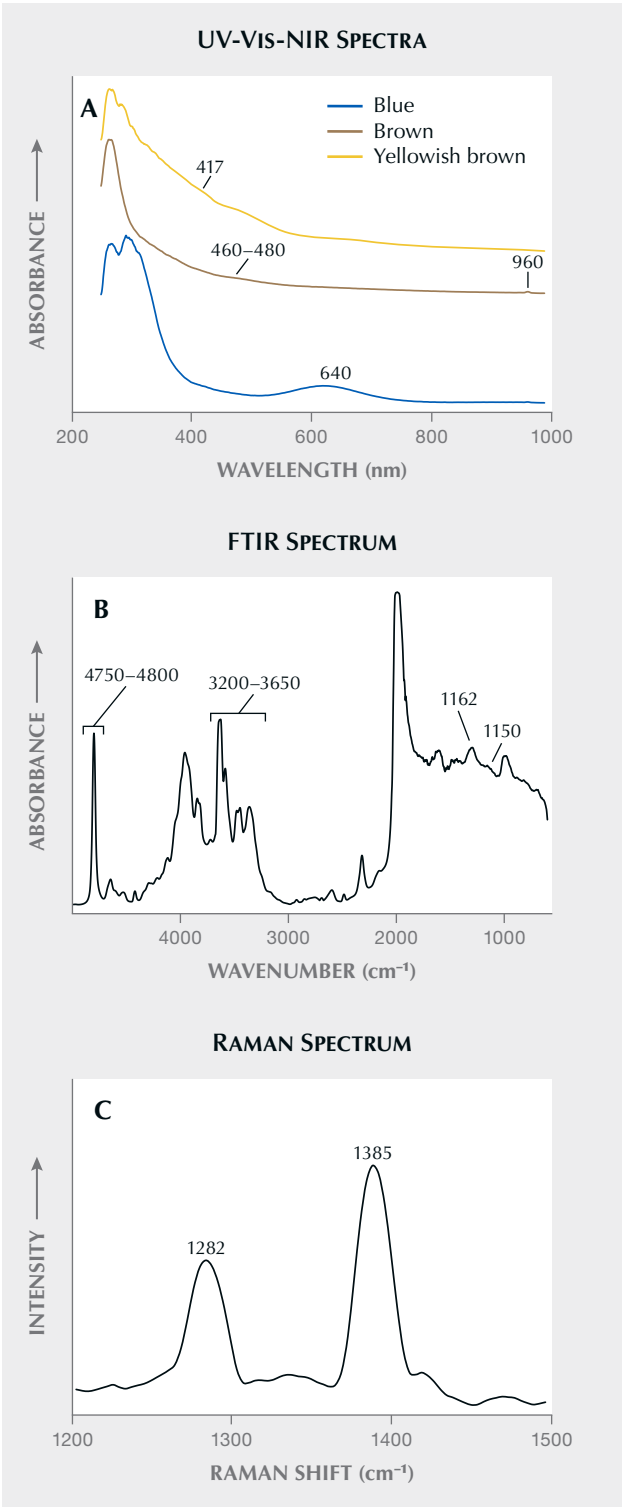

Figure 8. Representative UV-Vis-NIR, FTIR, and Raman spectra collected from 54 Texas topaz samples. The UV-Vis-NIR spectra were selected based on the prominence of the 417 nm, 460–480 nm, and 960 nm absorbances. The spectra are nonpolarized for the anisotropic topaz. Spectra are offset vertically for clarity. The Raman spectrum shows peaks related to CO_2.

lyzed Texas topaz had a small broad band at 640 nm (figure 8A). This feature has previously been attributed to an oxygen hole center that is strongly associated with the preservation of blue color (Krambrock et al., 2007). About 17% of the samples displayed a small broad band in the 460–480 nm range, likely associated with a temperature-sensitive oxygen hole center that causes brown color (Petrov, 1983; Aines and Rossman, 1986; Souza et al., 2006). Topaz with a broad 640 nm band sometimes has a 460–480 nm band, suggesting the two may be related. Small absorption bands at 417 nm occurred in 6% of the examined Texas topaz and indicate the presence of yellow color (Rossman, 2011). The defects responsible for the 417 nm absorption may be caused by a combination of a trapped-electron and oxygen hole centers (Schott et al., 2003; Gaft et al., 2005).

Each sample had a small absorbance peak at 960 nm, possibly an overtone of a hydroxyl (OH) group. Each topaz also had a large absorbance in the 230–305 nm range, likely produced by an Al=Si=O structure, which is an absorbance feature also observed in spodumene (Bonventi et al., 2012). Infrared absorbance in the 800–1050 cm^{-1} range is caused by vibrations of the SiO_4 tetrahedra, while observed absorbances near 1150 and 1162 cm^{-1} are commonly attributed to Al-OH and Al-O-H bonds within topaz (Londos et al., 1992; Prasad and Gowd, 2003; figure 8B). Absorbances observed in all samples occurring at 3200–3650 cm^{-1} and 4750–4800 cm^{-1} represented hydroxyl stretching vibrations (Aines and Rossman, 1986; Shinoda and Aikawa, 1997; Prasad and Gowd, 2003). Typically, OH substitutes for fluorine according to a temperature-dependent relationship in which higher OH correlates with crystallization at lower temperatures of 300–600°C compared to magmatic topaz formed at 600–800°C (Soufi, 2021 and references therein). No calibrations exist between IR absorbance and OH content in topaz, and therefore we did not establish absolute OH or fluorine content in Texas topaz. Regardless, most gem-quality topaz has high fluorine and low OH concentrations (G. Rossman, pers. comm., 2023), and the topaz-bearing pegmatites in Mason County host significant amounts of the fluorine-rich mineral fluorite (CaF_2).

Texas topaz is not typically free of inclusions. Only about 10% of the material is suitable for faceting when considering size, depth of color, color zoning, and inclusions. We occasionally observed multiphase fluid and melt inclusions, some containing bubbles of carbon dioxide. Among the mineral inclusions identified with Raman were albite,

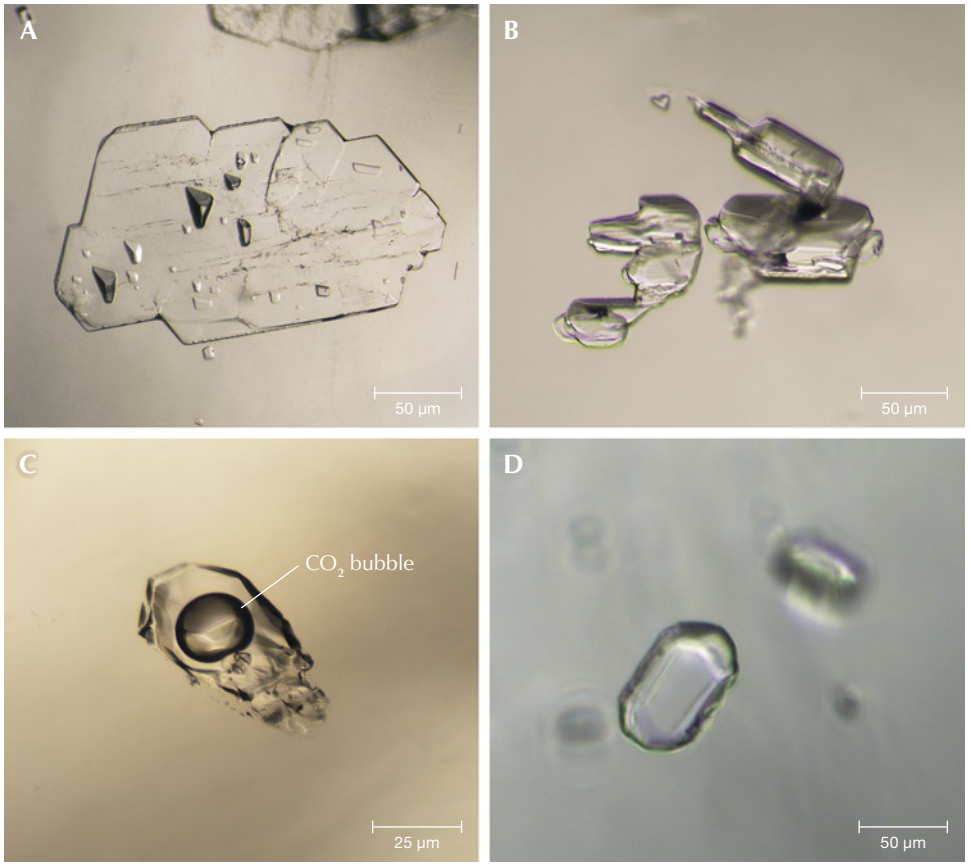

Figure 9. Examples of mineral and fluid inclusions found in Texas topaz: anorthosite (A), albite (B), fluid and melt inclusions (C), and quartz (D). Photomicrographs by Roy Bassoo.

anorthite, quartz, muscovite, pseudobrookite, rutile, and columbite-tantalite group minerals (figure 9). Most Texas topaz is alluvial and has been rounded by weathering. The waterworn samples had the fewest inclusions, which is expected because weathering in an alluvial environment would preferentially remove the poorer-quality stones by erosive attrition. For this reason, alluvial stones yield relatively flawless gemstones when faceted (Leiper, 1951).

Visual inspection and spectroscopic measurements revealed that Texas topaz shares many characteristics with topaz found in other localities globally. This study did not determine any defining characteristics or spectroscopic fingerprint to distinguish or differentiate Texas topaz.

Major and Trace Element Compositions. The major oxide composition of Texas topaz showed little deviation from that expected for $Al_2SiO_4(F,OH)_2$, with Al_2O_3 and SiO_2 accounting for 55.3 ± 0.4 wt.% and 31.8 ± 2.3 wt.%, respectively. The fluorine content of Texas topaz ranges from 19 to 21 wt.% (Collins, 2008), which suggests it may have formed from transitional pegmatite to hydrothermal processes (e.g., Foord et al., 1990; Soufi, 2021 and references therein). Minor oxide concentrations of FeO, MnO, and CaO were low, ranging from below detection limits to 0.3 wt.%. These major and minor element concentrations do not allow a clear distinction of Texas topaz from other global sources.

To test whether the trace element composition of Texas topaz has a characteristic identity, we measured trace elements in the samples. Germanium, iron, titanium, gallium, scandium, and phosphorus were detected consistently but at low concentrations (<600 ppm). Niobium, tantalum, tungsten, and tin were infrequently detected and when detected had very low concentrations (<5 ppm) (table 1). Similarly, the potential chromophore chromium was detected in only six samples but had a mean concentration of 27 ± 24 ppm.

Simple inspection of the trace element concentrations revealed limited diagnostic criteria. As expected with pegmatites, evidence of crystallization from highly fractionated fluids was present. Specifically, the niobium/tantalum (Nb/Ta) ratio of <5 served as a marker of mineralization in granitic rocks and can track increasing fractionation. This ratio likely reflects the magmatic to hydrothermal transition where tantalum is much less soluble than niobium in highly

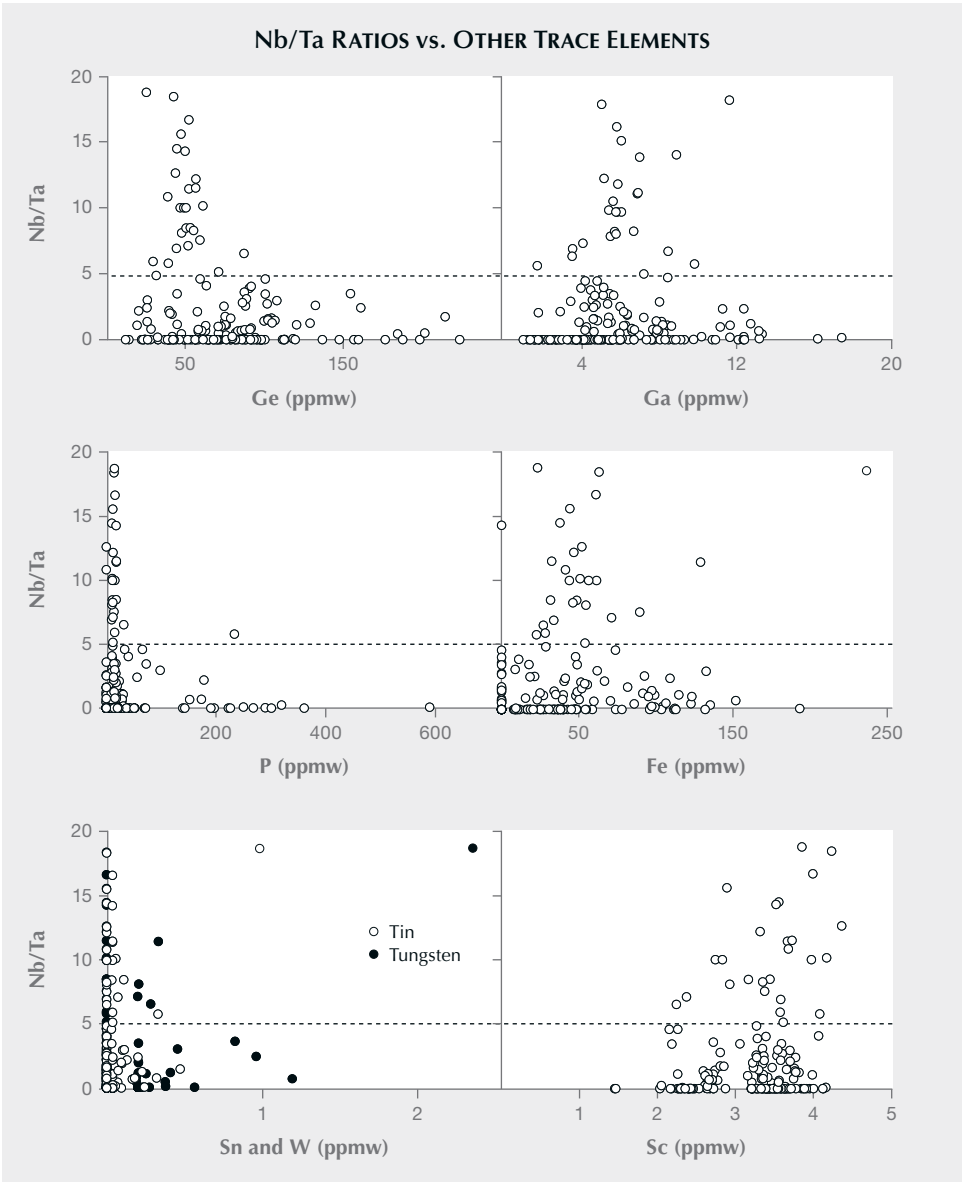

Figure 10. Nb/Ta ratios vs. germanium, gallium, phosphorus, iron, tin, tungsten, and scandium concentrations in Mason topaz. The dashed line indicates Nb/Ta ratios of ~5 (see Ballouard et al., 2016).

fractionated aqueous solutions (Zaraisky et al., 2010; Ballouard et al., 2016). Although the Nb/Ta ratio is normally applied to whole-rock analyses, germanium, gallium, phosphorus, tin, tungsten, and iron of the topaz samples showed increasing concentrations correlating with low Nb/Ta ratios (figure 10). Furthermore, most samples had gallium contents <20 ppm, but germanium ranged from 10 to 235 ppm. Such values are associated with topaz crystallization from pegmatites and greisens, consistent with the local Mason County geology (Duck, 1986; Breiter et al., 2013). Scandium concentration decreased with increasing fractionation, suggesting that scandium was incorporated into thortveitite or zinnwaldite during early crystallization of the host granite (Bianchi et al., 1988; Hreus et al., 2021). The concentrations of tin and tungsten were <3 ppm and notably low. However, the highly incompatible nature of tin and tungsten and the presence of cassiterite and scheelite in the region may collectively suggest greisen ore mineralization in Mason County (Paige, 1911; Meyer, 1913; Pollard et al., 1989). Indeed, previous geochemical studies suggest that topaz may indicate rare metal mineralization of pegmatites (Agangi et al., 2014, 2016).

The trace element concentrations of Texas topaz did not offer a readily accessible statistical or graphical signature for determining its origin. However, recent advances in machine learning as applied to trace

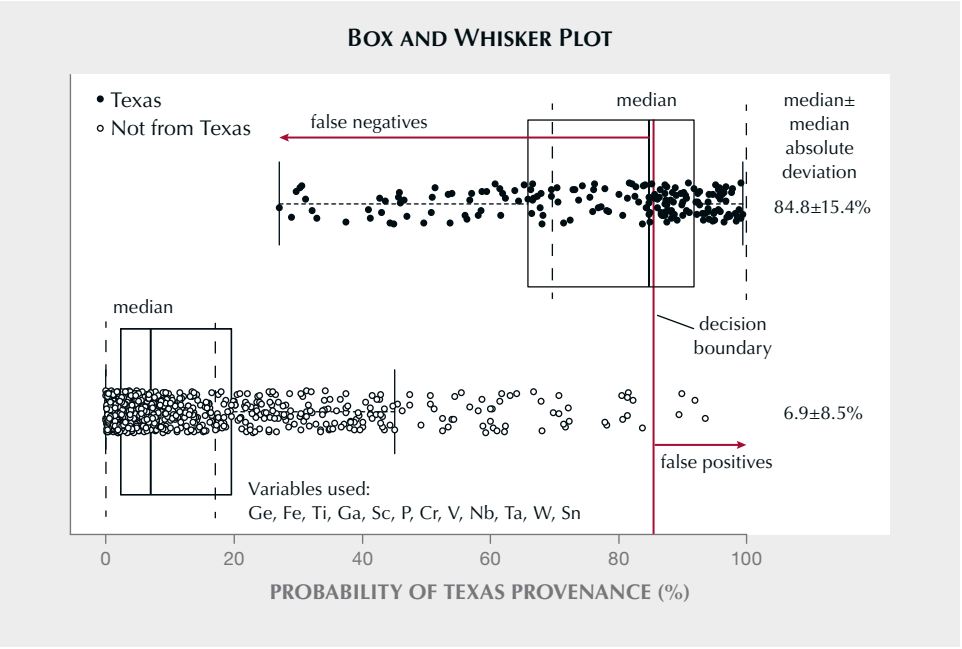

Figure 11. Box and whisker plot for the probability of Texas provenance for all topaz in this study, determined by the random forest machine learning method. Thick black vertical lines correspond to the median value, boxes correspond to the interquartile range (IQR), and horizontal dashed lines correspond to "whiskers" and extend 1.5× beyond the IQR. Samples with probabilities beyond the whiskers are considered outliers. The median absolute deviations are shown as vertical dashed lines.

element concentrations are a promising new tool for determining gemstone provenance. This approach is not without precedent for gemstones (e.g., Blodgett and Shen, 2011; Luo et al., 2015). We hypothesized that machine learning using the random forest statistical method could provide a robust probability of a specific topaz specimen being sourced from Mason County, Texas (Breiman, 2001). The effectiveness of machine learning depends in part on the size of the database available for model calibration, where larger datasets improve the effectiveness of the machine learning method. In this study, the authors compiled a new trace element dataset for 461 topaz samples, with 83 of known Texas provenance. However, it must be noted that Texas topaz are D-type and E-type samples according to GIA's origin classification scheme and were not obtained by sampling *in situ* (Vertriest et al., 2019).

To calibrate this model, the concentrations of germanium, iron, titanium, gallium, scandium, phosphorus, chromium, vanadium, niobium, tantalum, tungsten, and tin were used as variables. Each topaz could be assigned a pseudo-probability value by considering the proportion of the trees in the random forest model that "vote" for each outcome. Classification probability ranges from 0 to 100%, with higher probabilities indicating an increased likelihood of Texas provenance. One outcome was labeled "Texas" and the other "Not from Texas." The most significant trace elements for the Texas provenance were scandium, titanium, germanium, and chromium. An 85% decision boundary or classification value, above and below which one classifies a sample into different groups, was selected. Choosing the position of the decision boundary is user-determined and essential for making reliable provenance determinations (see appendix 1). Using these criteria, most topaz from Texas plotted with a very high likelihood of Texas origin (figure 11). Only ~12% of the 83 known Texas topaz samples were assigned a provenance other than Texas, or a "False Negative." These "False Negative" samples may correspond to populations that differ compositionally from the majority of Texas topaz. Regarding the overlap of probability, we find that some topaz from other locations has a higher probability of being derived from Texas, suggesting some degree of compositional similarity. This is expected in natural systems that have a continuum of compositional variability. However, analyzing additional Mason County samples will enable the model to better predict the provenance for these topaz compositions.

Importantly, 7% of the topaz from the global dataset were incorrectly classified as from Texas. These "False Positives" would be misidentified as "Texas" using the current machine learning approach. Samples from Namibia, Nigeria, Australia, and from California and Indiana in the United States were the most common false positives, with probabilities for Texas provenance of approximately 73%, 62%, 65%, 55%, and 70%, respectively (table 2). The ambiguity in our machine learning results was

TABLE 2. Median probabilities (±1σ)[a] or likelihood of topaz from other global locations being derived from Texas.

Locality	Tectonic environment[b]	No. of samples	Median probability of Texas provenance (%)
Germany	Extended crust	6	9 ± 9
Australia	Orogen	15	65 ± 28
Japan	Orogen	2	44 ± 7
Mexico	Orogen	80	3 ± 6
Pakistan	Orogen	10	6 ± 3
Russia	Orogen	18	1 ± 1
U.S. (California)	Orogen	5	55 ± 19
U.S. (Indiana)	Orogen	2	69 ± 2
Zimbabwe	Orogen	58	10 ± 6
Brazil	Shield	198	7 ± 5
Colombia	Shield	98	21 ± 12
Guyana	Shield	165	4 ± 3
Namibia	Shield	6	73 ± 8
Nigeria	Shield	10	62 ± 17
Sri Lanka	Shield	8	34 ± 19
U.S. (Colorado)	Shield	2	39 ± 4
U.S. (Utah)	Shield	50	3 ± 7

[a]*Includes replicate analyses. Please see appendix 1.*
[b]*Classes derived from Simmons et al. (2012).*

caused by fewer specimens from those locations. Larger sample sizes lead to more representative datasets. Greater sampling is required for populations where the compositional variation is larger. By acquiring more samples, we can better characterize the full compositional range of that suite of samples. For example, for populations of topaz with a smaller compositional range, fewer samples will be required to fully characterize the compositions of topaz from that locality. Indeed, countries with large numbers of topaz samples in this study, such as Brazil, Guyana, Colombia, Zimbabwe, and Mexico, had the lowest probabilities of Texas provenance, ranging from 3 to 21%.

These findings indicate that most Texas topaz have sufficiently distinct trace element compositions that allow them to be geochemically differentiated from topaz those in other global localities. Increased certainty in assigning provenance could be accomplished by also considering factors such as hue and saturation, fluorescence color, infrared and UV-Vis-NIR spectra, and inclusion suites (e.g., Palke et al., 2023). The machine learning model can also help identify deposits with similar geologic settings. The high predicted probability of similarity between Texas topaz and that from other U.S. locations and Australia may also indicate that they formed in similar geological conditions, resulting in the overlapping trace element compositions observed. Future studies of trace elements of tin and tungsten in topaz could improve our understanding of the geologic conditions leading to the formation of rare metal ore deposits, for example. Indeed, trace element compositions in colored stones better reflect the geologic environment in which they formed rather than their geographic origin (e.g., McClure et al., 2019).

CONCLUSIONS

Trace element compositions suggest topaz is derived from greisens and pegmatites. Furthermore, the presence of tin- and tungsten-bearing minerals such as cassiterite and scheelite, respectively, in the region

Figure 12. This 1,296 ct topaz crystal with a blue rim was recovered in Mason County, Texas. Photo by Ken Larsen; courtesy of the Smithsonian Institution Collection.

may collectively suggest greisen ore mineralization in Mason County. Topaz found in Mason County, Texas, has gemological characteristics that make it appealing for the gem trade (figure 12) and of particular commercial value throughout the state of Texas. However, misrepresentation often goes along with increased value. By combining trace element composition analysis with novel machine learning methods, origin determination for topaz could be possible. Better prediction of topaz provenance requires abundant sampling, especially from localities where current sampling is limited. This study has shown that trace element composition can be combined with traditional gemological observations to estimate a probability of Texas provenance. The inherent gemological value of Texas topaz is elevated by its domestic provenance, cementing its place among other highly prized gemstones from the United States.

ABOUT THE AUTHORS

Dr. Roy Bassoo is formerly a postdoctoral research associate at GIA in Carlsbad, California. Diane Eames is a GIA graduate gemologist and jeweler. Dr. Kenneth Befus is a gem and mineral curator at the Jackson School of Geosciences at University of Texas at Austin. Dr. Matthew F. Hardman is a research scientist at GIA in Carlsbad, California. Ziyun Sun is a senior research associate at GIA in Carlsbad, California.

ACKNOWLEDGMENTS

We sincerely thank Rose Tozer of GIA's Richard T. Liddicoat Gemological Library and Information Center for guiding us to excellent historical documents referring to Texas topaz. We also thank Dr. Aaron Palke for his technical feedback in the drafting of this article, Maxwell Hain for his philosophical contributions, Dr. Rhiana Elizabeth Henry for her proofreading, and the peer reviewers for feedback that improved the content of this article.

REFERENCES

Agangi A., Kamenetsky V.S., Hofmann A., Przybyłowicz W., Vladykin N.V. (2014) Crystallisation of magmatic topaz and implications for Nb-Ta-W mineralisation in F-rich silicic melts – The Ary-Bulak ongonite massif. *Lithos*, Vol. 202-203, pp. 317–330, http://dx.doi.org/10.1016/j.lithos.2014.05.032

Agangi A., Gucsik A., Nishido H., Ninagawa K., Kamenetsky V.S. (2016) Relation between cathodoluminescence and trace-element distribution of magmatic topaz from the Ary-Bulak massif, Russia. *Mineralogical Magazine*, Vol. 80, No. 5, pp. 881–899, http://dx.doi.org/10.1180/minmag.2016.080.023

Aines R.D., Rossman G.R. (1986) Relationships between radiation damage and trace water in zircon, quartz, and topaz. *American Mineralogist*, Vol. 71, No. 9-10, pp. 1186–1193.

Ballouard C., Poujol M., Boulvais P., Branquet Y., Tartèse R., Vigneresse J-L. (2016) Nb-Ta fractionation in peraluminous granites: A marker of the magmatic-hydrothermal transition. *Geology*, Vol. 44, No. 3, pp. 231–234, http://dx.doi.org/10.1130/G37475.1

Barker D.S., Reed R.M. (2010) Proterozoic granites of the Llano Uplift, Texas: A collision-related suite containing rapakivi and topaz granites. *Geological Society of America Bulletin*, Vol. 122, No. 1-2, pp. 253–264, http://dx.doi.org/10.1130/B26451.1

Barnes V.E., Hartmann B.M., Scranton D.F. (1992) Geologic Map of Texas: scale 1:500,000. Bureau of Economic Geology. University of Texas, Austin.

Bianchi R., Pilati T., Diella V., Gramaccioli C.M., Mannucci G. (1988) A re-examination of thortveitite. *American Mineralogist*, Vol. 73, No. 5-6, pp. 601–607.

Blodgett T., Shen A.H. (2011) Application of discriminant analysis in gemology: Country-of-origin separation in colored stones and distinguishing HPHT-treated diamonds. *G&G*, Vol. 47, No. 2, p. 145.

Bonventi W., Isotani S., Albuquerque A.R.P. (2012) Color dependence on thickness in topaz crystal from Brazil. *Advances in Condensed Matter Physics*, article no. 873804, http://dx.doi.org/10.1155/2012/873804

Breiman L. (2001) Random forests. *Machine Learning*, Vol. 45, pp. 5–32.

Breiter K., Gardenová N., Vaculovič T., Kanický V. (2013) Topaz as an important host for Ge in granites and greisens. *Mineralogical Magazine*, Vol. 77, No. 4, pp. 403–417, http://dx.doi.org/10.1180/minmag.2013.077.4.01

Browne V. (1982) Topaz in the Lone Star state. *Jewelry Making Gems and Minerals*, Vol. 531, pp. 16–18.

Burt D.M., Sheridan M.F., Bikun J.V., Christiansen E.H. (1982) Topaz rhyolites; distribution, origin, and significance for exploration. *Economic Geology*, Vol. 77, No. 8, pp. 1818–1836, http://dx.doi.org/10.2113/gsecongeo.77.8.1818

Charoy B., Noronha, F. (1996) Multistage growth of a rare-element, volatile-rich microgranite at Argemela (Portugal). *Journal of Petrology*, Vol. 37, No. 1, pp. 73–94, http://dx.doi.org/10.1093/petrology/37.1.73

Collins A. (2008) Chemical and optical discriminators for Mason topaz. Undergraduate senior honors thesis, University of Texas, Austin.

Congdon R.D., Nash W.P. (1988) High-fluorine rhyolite: An eruptive pegmatite magma at the Honeycomb Hills, Utah. *Geology*, Vol. 16, No. 11, pp. 1018–1021, http://dx.doi.org/10.1130/0091-7613(1988)016%3C1018:HFRAEP%3E2.3.CO;2

Crowningshield R. (1981) Irradiated topaz and radioactivity. *G&G*, Vol. 17, No. 4, pp. 215–217.

Duck J.J. (1986) Investigation of factors controlling the partitioning of trace germanium and gallium between topaz and quartz. PhD thesis, University of Pittsburgh.

Fechenbach M.F. (1984) Trapping the crafty topaz. *Jewelry Making Gems and Minerals*, Vol. 558, pp. 55–57.

Foord E.E., Jackson L.L., Taggart J.E., Crock J.G., King T.V.V. (1990) Environment of crystallization of topaz as inferred from crystal chemistry and infrared spectra. In *Abstracts of the 15th General Meeting of the International Mineralogical Association Proceedings*, pp. 306–307, Beijing.

Gaft M., Nagli L., Reisfeld R., Panczer G., Brestel M. (2003) Time-resolved luminescence of Cr^{3+} in topaz $Al_2SiO_4(OH,F)_2$. *Journal of Luminescence*, Vol. 102-103, pp. 349–356, http://dx.doi.org/10.1016/S0022-2313(02)00532-X

Gaft M., Reisfeld R., Panczer G. (2005) *Modern Luminescence Spectroscopy of Minerals and Materials*. Springer Berlin, Heidelberg, 356 pp.

Gauzzi T., Graça L.M. (2018) A cathodoluminescence-assisted LA-ICP-MS study of topaz from different geological settings. *Brazilian Journal of Geology*, Vol. 48, No. 01, pp. 161–176, http://dx.doi.org/10.1590/2317-4889201820170127

Gauzzi T., Graça L.M., Lagoeiro L., de Castro Mendes I., Queiroga G.N. (2018) The fingerprint of imperial topaz from Ouro Preto region (Minas Gerais state, Brazil) based on cathodoluminescence properties and composition. *Mineralogical Magazine*, Vol. 82, No. 4, pp. 943–960, http://dx.doi.org/10.1180/minmag.2017.081.078

Hinton J.J. (2005) *Communities and Small-Scale Mining: An Integrated Review for Development Planning*. CASM, Washington, DC.

Hoover D.B. (1992) *Topaz*. Butterworth-Heinemann Ltd., London.

Hreus S., Výravský J., Cempírek J., Breiter K., Galiová M.V., Krátký O., Šešulka V., Škoda R. (2021) Scandium distribution in the world-class Li-Sn-W Cínovec greisen-type deposit: Result of a complex magmatic to hydrothermal evolution, implications for scandium valorization. *Ore Geology Reviews*, Vol. 139, Part A, article no. 104433, http://dx.doi.org/10.1016/j.oregeorev.2021.104433

International Labour Organization (1999) Social and labour issues in small-scale mines. Report at the Tripartite Meeting on Social and Labour Issues in Small-Scale Mines, ILO, Geneva.

King Jr. E.A. (1961) Texas gemstones. Bureau of Economic Geology, Report of Investigations, No 42. The University of Texas at Austin, Austin, Texas.

Krambrock K., Ribeiro L.G.M., Pinheiro M.V.B., Leal A.S., Menezes M.Â de B.C., Spaeth J.-M. (2007) Color centers in topaz: Comparison between neutron and gamma irradiation. *Physics and Chemistry of Minerals*, Vol. 34, pp. 437–444, http://dx.doi.org/10.1007/s00269-007-0160-z

Kunz G.F. (1893) Notes on topaz from Texas. *New York Academy of Science Transactions*, Vol. 12, p. 96.

Lafuente B., Downs R.T., Yang H., Stone N. (2016) The power of databases: The RRUFF project. In T. Armbruster and R.M. Danisi, Eds., *Highlights in Mineralogical Crystallography*, pp. 1–29. W. de Gruyter GmbH, Berlin.

Leiper H. (1951) Texas blue topaz. *Lapidary Journal*, Vol. 5, No. 1, pp. 98–102.

Londos C.A., Vassilikou-Dova A., Georgiou G., Fytros L. (1992) Infrared studies of natural topaz, *Physica Status Solidi A*, Vol. 133, No. 2, pp. 473–479, http://dx.doi.org/10.1002/pssa.2211330231

Luo Z., Yang M., Shen A.H. (2015) Origin determination of dolomite-related white nephrite through iterative-binary linear discriminant analysis. *G&G*, Vol. 51, No. 3, pp. 300–311, http://dx.doi.org/10.5741/GEMS.51.3.300

Manning D.A.C., Hill P.I. (1990) The petrogenetic and metallogenetic significance of topaz granite from the southwest England orefield. In H.J. Stein and J.L. Hannah, Eds., *Orebearing Granite Systems; Petrogenesis and Mineralizing Processes*, Vol. 246, Geological Society of America, Boulder, Colorado, http://dx.doi.org/10.1130/SPE246-p51

Marshall D., Walton L. (2007) Topaz. In L.A. Groat, Ed., *Geology of Gem Deposits*. Mineralogical Association of Canada Short Course Series, Vol. 37, pp. 161–168.

McClure S.F., Moses T.M, Shigley J.E. (2019) The geographic origin dilemma. *G&G*, Vol., 55, No. 4, pp. 457–462.

Menzies M.A. (1995) The mineralogy, geology and occurrence of

topaz. *Mineralogical Record*, Vol. 26, No. 1, pp. 5–53.
Meyer L.C. (1913) Topaz and stream tin in Mason County, Texas. *Engineering and Mining Journal*, Vol. 95, pp. 511–512.
Mosher S., Levine J.S.F., Carlson W.D. (2008) Mesoproterozoic plate tectonics: A collisional model for the Grenville-aged orogenic belt in the Llano uplift, central Texas. *Geology*, Vol. 36, No. 1, pp. 55–58, http://dx.doi.org/10.1130/G24049A.1
Nassau K. (1985) Altering the color of topaz. *G&G*, Vol. 21, No. 1, pp. 26–34, http://dx.doi.org/10.5741/GEMS.21.1.26
Nassau K., Prescott B.E. (1975) Blue and brown topaz produced by gamma irradiation. *American Mineralogist*, Vol. 60, No. 7-8, pp. 705–709.
Paige S. (1911) Mineral resources of the Llano-Burnet region, Texas, with an account of the Precambrian geology. U.S. Department of the Interior, Bulletin 450.
Palke A., Renfro N., Hapeman J.R., Berg R.B. (2023) Gemological characterization of Montana sapphire from the secondary deposits at Rock Creek, Missouri River, and Dry Cottonwood Creek. *G&G*, Vol. 59, No. 1, pp. 2–45, http://dx.doi.org/10.5741/GEMS.59.1.2
Payette C., Martin R.F. (1990) Melt inclusions in the quartz phenocrysts of rhyolites from Topaz and Keg Mountains, Thomas Range, Utah. *Geological Society of America Special Papers*, Vol. 246, pp. 89–102.
Petrov I. (1983) Paramagnetische Zentren in Topas. PhD thesis, Heidelberg University, Germany.
Petrov I., Beredinski W., Bank H. (1977) Bestrahlte gelbe und rotbraune Topase and ihre Erkennung. *Zeitschrift der Deutschen Gemmologischen Gesellschaft*, Vol. 26, No. 3, pp. 148–151.
Pollard P.J., Taylor R.G., Tate N.M. (1989) Textural evidence for quartz and feldspar dissolution as a mechanism of formation for Maggs pipe, Zaaiplaats tin mine, South Africa. *Mineralium Deposita*, Vol. 24, No. 3, pp. 210–218, http://dx.doi.org/10.1007/BF00206444
Pough F.H. (1957) The coloration of gemstones by electron bombardment. *Zeitschrift der Deutschen Gesellschaft für Edelsteinkunde*, Vol. 20, p. 71.
Prasad P.S.R., Gowd T.N. (2003) FTIR spectroscopic study of hydroxyl ions in natural topaz. *Journal Geological Society of India*, Vol. 61, pp. 202–208.
Reed R.M. (1999) Emplacement and deformation of late syn-orogenic, Grenville-age granites in the Llano Uplift, Central Texas. PhD thesis, University of Texas, Austin.
Raimbault L., Cuney M., Azencott C., Duthou J.-L., Joron J.L. (1995) Geochemical evidence for a multistage magmatic genesis of Ta-Sn-Li mineralization in the granite at Beauvoir, French Massif Central. *Economic Geology*, Vol. 90, No. 3, pp. 548–576, http://dx.doi.org/10.2113/gsecongeo.90.3.548
Rossman G.R. (2011) The color of topaz. In *Topaz: Perfect Cleavage*. ExtraLapis English. No. 14. Lithographie, LLC, Denver, Colorado, pp. 79–85.
Schott S., Rager H., Schürmann K., Taran M. (2003) Spectroscopic study of natural gem quality "Imperial"-topazes from Ouro Preto, Brazil. *European Journal of Mineralogy*, Vol. 15, No. 4, pp. 701–706, http://dx.doi.org/10.1127/0935-1221/2003/0015-0701
Shinoda K., Aikawa N. (1997) IR active orientation of OH bending mode in topaz. *Physics and Chemistry of Minerals*, Vol. 24, No. 8, pp. 551–554, http://dx.doi.org/10.1007/s002690050071
Simmons W.B. (2007) Gem-bearing pegmatites. In L.A. Groat, Ed., *Geology of Gem Deposits*. Mineralogical Association of Canada Short Course Series, Vol. 37, pp. 169–206.
Simmons W.B., Pezzotta F., Shigley J.E., Beurlen H. (2012) Granitic pegmatites as sources of colored gemstones. *Elements*, Vol. 8, No. 4, pp. 281–287, http://dx.doi.org/10.2113/gselements.8.4.281
Sinkankas J. (1997) *Gemstones of North America, Volume 3*. Geoscience Press, Inc., Tucson, Arizona.
Smith A.E. (2008) The Baringer Hill pegmatite, Llano County, Texas. *The Backender's Gazette*, September, pp. 6–18.
Soufi M. (2021) Origin and physical-chemical control of topaz crystallization in felsic igneous rocks: Contrasted effect of temperature on its OH–F substitution. *Earth Science Reviews*, Vol. 213, article no. 103467, http://dx.doi.org/10.1016/j.earscirev.2020.103467
Souza D.N., Fernandes de Lima J., Valerio M.E.G., Caldas L.V.E. (2006) Thermally stimulated luminescence and EPR studies on topaz. *Applied Radiation and Isotopes*, Vol. 64, No. 8, pp. 906–909, http://dx.doi.org/10.1016/j.apradiso.2006.03.006
Sparks D. (1968) The Texas topaz fields. *Gems and Minerals*, Vol. 367, pp. 20–25.
Taran M.N., Langer K., Platonov A.N., Indutny V. (1994) Optical absorption investigation of Cr^{3+} ion-bearing minerals in the temperature range 77-797 K. *Physics and Chemistry of Minerals*, Vol. 21, No. 6, pp. 360–372, http://dx.doi.org/10.1007/BF00203294
Taran M.N., Tarashchan A.N., Rager H., Schott St., Schürmann K., Iwanuch W. (2003) Optical spectroscopy study of variously colored gem-quality topazes from Ouro Preto, Minas Gerais, Brazil. *Physics and Chemistry of Minerals*, Vol. 30, No. 9, pp. 546–555, http://dx.doi.org/10.1007/s00269-003-0356-9
Taylor R.P. (1992) Petrological and geochemical characteristics of the Pleasant Ridge zinnwaldite-topaz granite, southern New Brunswick, and comparisons with other topaz-bearing felsic rocks. *Canadian Mineralogist*, Vol. 30, No. 3, pp. 895–921.
Towner J.M. (1968) A topaz hunt in Mason County, Texas. *Lapidary Journal*, September, pp. 780–785.
——— (1969) Bigger and better topaz in Mason County. *Lapidary Journal*, August, pp. 700–705.
Vertriest W., Palke A.C., Renfro N.D. (2019) Field gemology: Building a research collection and understanding the development of gem deposits. *G&G*, Vol. 55, No. 4, pp. 490–511, http://dx.doi.org/10.5741/GEMS.55.4.490
White J.W. (1960) Topaz-bearing pegmatites and gem topaz in the Llano Uplift, Texas. Master's thesis, University of Texas, Austin.
Williams-Jones A.E., Samson I.M., Olivo G.R. (2000) The genesis of hydrothermal fluorite-REE deposits in the Gallinas Mountains, New Mexico. *Economic Geology*, Vol. 95, No. 2, pp. 327–341, http://dx.doi.org/10.2113/gsecongeo.95.2.327
Worden P.W. Jr. (1977) Lone Star. *Facets*, February, p. 4.
Zaraisky G.P., Korzhinskaya V., Kotova N. (2010) Experimental studies of Ta_2O_5 and columbite–tantalite solubility in fluoride solutions from 300 to 550°C and 50 to 100 MPa. *Mineralogy and Petrology*, Vol. 99, pp. 287–300, http://dx.doi.org/10.1007/s00710-010-0112-z
Zhang R.Y., Liou J.G., Shu J.F. (2002) Hydroxyl-rich topaz in high-pressure and ultrahigh-pressure kyanite quartzites, with retrograde woodhouseite, from the Sulu terrane, eastern China. *American Mineralogist*, Vol. 87, No. 4, pp. 445–453, http://dx.doi.org/10.2138/am-2002-0408